ACS APPLIED MATERIALS & INTERFACES

Research Article

www.acsami.org

Multipurpose Ultra and Superhydrophobic Surfaces Based on Oligodimethylsiloxane-Modified Nanosilica

Raquel de Francisco,[†] Pilar Tiemblo,*[,†] Mario Hoyos,[†] Camino González-Arellano,[†,⊥] Nuria García,*[,†] Lars Berglund,[‡] and Alla Synytska[§,∥]

[†]Instituto de Ciencia y Tecnología de Polímeros, ICTP-CSIC, Juan de la Cierva 3, 28006 Madrid, Spain

[‡]Wallenberg Wood Science Center, KTH Royal Institute of Technology, SE-10044 Stockholm, Sweden

[§]Leibniz-Institut für Polymerforschung Dresden e.V., Hohe Str. 6, D-01069 Dresden, Germany

[∥]Technische Universität Dresden, Physical Chemistry of Polymer Materials, 01062 Dresden, Germany

Supporting Information

ABSTRACT: Nonfluorinated hydrophobic surfaces are of interest for reduced cost, toxicity, and environmental problems. Searching for such surfaces together with versatile processing, A200 silica nanoparticles are modified with an oligodimethylsiloxane and used by themselves or with a polymer matrix. The goal of the surface modification is controlled aggregate size and stable suspensions. Characterization is done by NMR, microanalysis, nitrogen adsorption, and dynamic light scattering. The feasibility of the concept is then demonstrated. The silica aggregates are sprayed in a scalable process to form ultrahydrophobic and imperceptible coatings with surface topographies of controlled nanoscale roughness onto different supports, including nanofibrillated cellulose. To improve adhesion and wear properties, the organosilica was mixed with polymers. The resulting composite coatings are characterized by FE-SEM, AFM, and contact angle measurements. Depending on the nature of the polymer, different functionalities can be developed. Poly(methyl methacrylate) leads to almost superhydrophobic and highly transparent coatings. Composites based on commercial acrylic car paint show "pearl-bouncing" droplet behavior. A light-emitting polyfluorene is synthesized to prepare luminescent and water repellent coatings on different supports. The interactions between polymers and the organosilica influence coating roughness and are critical for wetting behavior. In summary, the feasibility of a facile, rapid, and fluorine-free hydrophobization concept was successfully demonstrated in multipurpose antiwetting applications.

KEYWORDS: *superhydrophobic, coating, organosilica, oligodimethylsiloxane*

1. INTRODUCTION

During the past decade, superhydrophobic surfaces have received much attention because of the challenge of understanding their basis[1−3] and the many technological implications they possess. Self-cleaning, antiicing, superslippery or antibiofouling surfaces can be developed from the same concept.[4−7] Most of the applications require coatings for large surfaces. This is a difficulty, since many strategies followed to hydrophobize surfaces are not easily applicable to large surface areas.[8] Therefore, a current target is to find suitable concepts for preparation and application of hydrophobic and mechanically stable coatings to large multipurpose areas. Furthermore, optical transparency[9] is an additional feature of great importance in many industrial applications. This property cocktail is an ambitious objective. This is why, in spite of the vast amount of literature devoted to superhydrophobicity, commercially available products are still limited. In particular, the difficulties associated with the surface roughness design are the most complicated to overcome.

Superhydrophobicity is based on the combination of low surface energy and suitable topography. Strictly speaking, the definition implies a water contact angle, θ_w, higher than 150° and, most importantly, a hysteresis, $\Delta\theta$, defined as the difference between advancing and receding water contact

Received: July 24, 2014
Accepted: October 2, 2014
Published: October 2, 2014

angles, lower than 10°. Provided $\Delta\theta < 10°$, a water drop will roll off the surface easily with a minimum tilt angle. The methodologies to build a superhydrophobic surface can be divided into those which lower the energy of a rough surface and those which induce roughness on a low energy surface. The former presents two main handicaps: the frequent use of fluorocompounds, and the complexity of employing methods involving two or more steps in large surface applications. With respect to surface roughening, common top-down approaches,[10] such as lithography may be restricted to small surfaces or specific applications. Finally, the self-assembly and sol−gel processes are probably the most promising and suitable approaches to meet all the requirements.[11]

Regarding topographic profile, a dual-scale roughness, with microstructures covered with nanometric entities, nicely exemplified by the Lotus leaf, was first thought to be needed for superhydrophobicity. However, biomimetic approaches are not usually as robust as natural patterns and in outdoor applications the microstructures are easily worn by environmental effects or mechanical wear.[12,13] In addition, the dual-size profile is frequently incompatible with optical transparency since the microstructures commonly have a size larger than the visible range wavelength.[14] Fortunately, it has been recently proven that a continuous nanoscale roughness may be enough to attain superhydrophobic behavior.[15] Single-scale profiles, although not trivial and requiring a precise size control, seem to be, a priori, more robust, better applicable and less demanding than multiple-scale ones.

The surface modification of nanoparticles provides an excellent platform to develop superhydrophobic coatings. One problem though is the strong and uncontrolled aggregation of the nanoparticles. Also, particle-based coatings tend to show poor mechanical stability. In previous work,[16,17] we showed that nanosilica aggregation can be controlled and tuned by an adequate choice of organic modifier, the modification method and the solvent used to prepare the organosilica suspension. Long modifier chains, chemically attached to the particle surface will lead to large particle agglomeration due to the occurrence of entanglements and organic bridges between aggregates. It is also shown that controlling the aggregate size of the organosilica in suspension enables one to adjust the surface roughness length scale of the coatings. This methodology was termed "chemically guided topography".[16]

With the aim of addressing the drawbacks mentioned so far (need for simple and scalable procedures apt for large surfaces, robust single scale topography and fluorine-free chemistry) we have oriented our research to a concept valid for imparting superhydrophobic behavior to a wide range of surfaces with a single, simple, scalable and fluorine-free process. For its success this concept relies, as key tools, on the "chemically guided topography" methodology and on the properties and morphology of a very specific organosilica aggregate. The goal of this work is not, then, the proposal of yet another superhydrophobic system,[18−20] but the demonstration of the multipurpose nature of this concept, based on the control and the stability in suspension of a particular organosilica aggregates.

Two methodologies are described in this work, (i) direct application of the organosilica suspension onto the surface of paper, glass, plastic or cellulose aerogels, which become ultra- or superhydrophobic and (ii) development of polymer based composite coatings, presenting both water repellency and mechanical stability. Among the composites, three polymer matrix examples are provided: poly(methyl methacrylate) (PMMA), a car paint based on acrylic polymers, and polyfluorene (PFO), a conjugated and light emitted polymer. As an added strength of the concept, in the silica/polymer coatings, water repellency is combined with other intrinsic functionalities of each polymer, such as optical transparency in PMMA or fluorescence in PFO.

2. EXPERIMENTAL SECTION

2.1. Materials. Hydrophilic fumed silica, A200, supplied by Degussa, silanol terminated oligodimethylsiloxane of 7 repeat units as average purchased from ABCR (PDMS-7), and PMMA (M_w = 120 000 g mol^{-1}) and methyltrimethoxysilane (MTMS) supplied by Sigma-Aldrich were used without further purification. Solvents for reactions, filtration, and chromatography were certified ACS grade and were purchased from Sigma-Aldrich. Certified ACS grade toluene (≥95%) was degassed with N_2 overnight, refluxed over Na, distilled under N_2 atmosphere and stored over regenerated 3 Å molecular sieves before using for polymerizations.[21] 9,9-Dioctyl-2,7-dibromofluorene, 9,9-dioctylfluorene-2,7-diboronic acid bis-(1,3-propanediol) ester, Aliquat 336, sodium carbonate (Na_2CO_3, 99.95%) and *tetrakis*(triphenylphosphine) palladium-(0) (99.9+%-Pd), $Pd(PPh_3)_4$, were purchased from Sigma-Aldrich.

A nonaqueous acrylic commercial car paint (Glasurit 22 from BASF Coatings) has been employed. The formulation is an acrylic resin, a pigment and the catalyst in a weight ratio 1.8:7.2:1 following the producer recipe. An acrylic solvent (10 wt %) was used as flow aid.

A nanofibrillated cellulose (NFC) water suspension was prepared from never-dried softwood sulphite pulp fibers (DP of 1200, lignin and hemicelluloses contents of 0.7 and 13.8%, respectively, Nordic Paper Seffle AB, Sweden) according to a previously reported method.[22] The pulp was first subjected to a pretreatment step involving enzymes and mechanical beating. Subsequently, the pretreated pulp was disintegrated by a mechanical homogenization process using a Microfluidizer M-110EH apparatus (Microfluidics, U.S.A.) so that a 2 wt % NFC suspension in water was obtained.

2.1.1. Synthesis of Poly(9,9′-dioctyl-9H-fluorene) (PFO). Inside a glovebox, 9,9′-dioctylfluorene-2,7-diboronic acid bis-(1,3-propanediol) ester (1.05 mmol, 0.586 g) and 9,9′-dioctyl-2,7-dibromofluorene (1 mmol, 0.548g) were dissolved in anhydrous toluene (16 mL), followed by the addition of the phase-transfer catalyst Aliquat 336 (0.1 mmol, 40.5 mg). Tetrakis(triphenylphosphine) palladium(0) (0.01 mmol, 11.56 mg) was dissolved in anhydrous toluene (2 mL) and then transferred into the aforementioned mixture. Outside the glovebox, a degassed Na_2CO_3 aqueous solution was syringed in through the septum. The reaction mixture was purged five times with nitrogen and refluxed under vigorous stirring at 100 °C for 12 h. Anhydrous toluene (1 mL) containing 4-bromobenzene, acting as the end-capping agent (in excess: 0.5 mmol) was then added, and the mixture was stirred continuously at 100 °C up to 24 h. The reaction was cooled to room temperature and polymers were precipitated from cold methanol, loaded onto a pad of silica and eluted by washing with dichloromethane. The solution was extracted with an aqueous sodium *N*,*N*-diethyldithiocarbamate solution (1 M) in order to remove the possible traces of Pd,[23] then water and dried over $MgSO_4$. After evaporation of the solvent, the

polymer was precipitated from a concentrated solution of dichloromethane into methanol and filtered off. The product was purified by four Soxhlet extractions cycles under nitrogen with methanol, hexane, acetone, and recovered from THF (1 day each). Final polymers were precipitated from methanol, filtered, and dried under vacuum at room temperature overnight. The light violet polymer particles thus obtained amounted to 0.328 g (yield: 85%) and, after the purification process, the total amount obtained was 0.243 g (63%). ^{1}H NMR (300 MHz, $CDCl_3$) d [ppm]: 7.784−7.596 (m, 6H, phenyl rings of fluorene), 7.486−7.104 (end-capper agent), 2.058 (s, 4H, 3-CH_2 of 9,9′-dioctylfluorene), 1.081 (s, 24H, 2-CH_2 of 9,9′-dioctylfluorene), and 0.781 (s, 6H, 1-CH_3 of 9,9′-dioctylfluorene).

2.1.2. Preparation of Organosilica (P^7). The surface modification of the silica was done by magnetically stirring for 72 h a mixture of A200 (3 g) and PDMS-7 (1.76 g) in 200 mL of toluene. The resulting organosilica, P^7, was isolated from the reaction medium by centrifugation and purified by means of repetitive washing in dichloromethane and acetone (3 times) and further centrifugation. The centrifugation process was carried out at 3500 rpm during 15 min. Finally, materials were dried at 100 °C overnight.

2.2. Preparation of Hydrophobic Coatings. *2.2.1. Particle-Only Coating.* P^7 suspension in isopropyl alcohol (IPA) at a concentration of 27 mg·mL^{-1} was stirred for 24 h before the deposition on a substrate (glass support, a PMMA film and a Whatman paper, grade 40, with nominal pore size of 8 μm) by spray coating with an airbrush AB931 from Sealey.

2.2.2. Hydrophobization of NFC. Before hydrophobization, the original cellulose dispersion was diluted ten times (0.13 wt %) and sonicated with a UP400S Hielscher during 3 cycles of 5 min long at 100 W. After that, the NFC were isolated by lyophilization and the resulting aerogel was immersed in dispersions of P^7 of different particle contents 3, 0.6, and 0.1 wt %. Immersion time was 30 s for the 3 and 0.6 wt % dispersions and 1 min for the 0.1 wt % one. The modified aerogels were then dried at room temperature for 12 h.

2.2.3. Composite Coatings. PMMA/P^7 coatings were prepared by adding 50 wt % P^7 particles from a previously stirred 2 wt % dispersion in toluene, to a 3 wt % PMMA solution in the same solvent. This mixture was magnetically stirring for other 24 h and after that, a controlled evaporation of the solvent (up to 20−25 wt % of toluene in the mixture) was carried out. The purpose of the controlled evaporation was to gradually increase the viscosity of the mixture while it was kept under stirring to maintain a good dispersion of the organosilica in the final mixture and prevent the deposition of the particles.[24] The blend was then sprayed on a glass support and a polyethylene (PE) film.

Self-cleaning paints were prepared by adding 50 wt % of P^7 to the commercial paint formulation. The mixture was magnetically stirring for 3 and 24 h and then was sprayed on glass supports by using the airbrush.

PFO composite coatings were prepared by dissolving the corresponding amount of PFO (2.8 wt %) in toluene (3 mL), to form homogeneous solutions to which a certain amount of P^7 was added (10, 30, or 50 wt % with respect to PFO). The suspensions were kept under stirring for 24 h. Then, a controlled evaporation of the solvent was carried out. Subsequently, the blends were sprayed on glass supports and cellulose based supports (HAWP02500 from Millipore with 0.45 μm of nominal pore and Whatman paper).

2.3. Characterization of the Organosilica and Coatings. The P^7 NMR spectra were performed in a Bruker Avance 400 spectrometer (Bruker Analytik GmbH Karlsrube, Germany) equipped with a Bruker Ultrashield 9.4 T (^{13}C and ^{29}Si frequencies of 100.62 and 79.49 MHz, respectively), 8.9 cm vertical-bore superconducting magnet. In both cases, ^{13}C and ^{29}Si, CP/MAS NMR spectra were acquired at ambient temperature by using a standard Bruker broad-band MAS probe. Representative samples were ground and packed in 4 mm zirconia rotors, sealed with Kel-F caps and spun at 5 kHz. The 90° pulse width was 3.5−4.5 μs and, in all cases, high-power proton decoupling was used. All free-induction decays were subjected to standard Fourier transformation and phasing. The chemical shifts were externally referenced to TMS. The ^{29}Si CP/MAS NMR spectrum was obtained with 4 ms CP contact time, 4 s recycle delay, 16 000 averages, and 80 Hz line broadening. ^{13}C CP/MAS NMR spectrum was acquired with 1 ms CP contact time, a 3 s recycle decay, 4500 averages and 200 Hz line broadening.

The organic mass (OM%) in P^7 was calculated from carbon content (C%) obtained by a LECO CHNS-932 equipment through the equation: OM% = (C% × 74)/24. BET surface area (S_{BET}) measurements were made by single-point nitrogen adsorption, using a Micromeritics Flowsorb 2300. The particle aggregate size, Z_{ave}, and the polydispersity index, Pdi, have been evaluated by dynamic light scattering (DLS) with a Zetasizer Nano ZS (Malvern Instruments) on suspension in IPA with a particle concentration of 50 μg mL^{-1}. The surface coating morphology was visualized by scanning electron microscopy (SEM) using a Philips XL30ESEM and a Hitachi SU-8000. Atomic force microscopy (AFM) was used to examine the surface topography. The AFM images (50 μm × 50 μm) were obtained with a Veeco Multimode scanning probe microscope equipped with a Nanoscope IV a controller operating in tapping mode with a phosphorus doped silicon cantilever (model RTESP). Mean square roughness values, Rq, were extracted from these images.

Contact angles were measured with Milli-Q grade water by the sessile drop method using a conventional drop shape analysis technique (Attension Theta optical tensiometer). For dynamic measurements (advancing and receding contact angles required to obtain $\Delta\theta$) the initial water drop volume was 5 μL and the volume was increased up to 10 μL by water disposal at 0.2 μL s^{-1} recording and analyzing 10 images per second during this process. A constant contact angle value is achieved, which is considered the advancing water contact angle. Then, 5 μL of water were removed at the same rate following identical analysis protocol what enables the determination of the receding contact angles. The determination of the contact angle from the captured images is done by the Young−Laplace method. If the water drop rolls off when the needle dispenser is removed, the $\Delta\theta$ value is considered as zero. $\Delta\theta$ values higher than 20° are difficult to quantify and meaningless in the context of this work. The initial water contact angle in static conditions with a 5 μL-volume drop is considered θ_w. Reported contact angles values were the average of at least five measurements in different coating regions.

3. RESULTS AND DISCUSSION

The starting point is preparation of an organosilica, termed P^7, from the well-known pyrogenic A200 nanosilica. Once modified, P^7 aggregates have very stable size and morphology,

Table 1. Characterization of P^7 Modified Silica Particles in the Form of Powder, IPA (Isopropyl Alcohol) Suspension, and Coating onto Glass Support[a]

				IPA suspension		coating		
sample	description	OM%	S_{BET} (m^2g^{-1})	Z_{ave} (nm)	Pdi	θ_w (deg)	$\Delta\theta$ (deg)	Rq50 (nm)
A200	raw silica		190	294 ± 9	0.13 ± 0.01	51 ± 1	>20	51
P^7	modified with PDMS-7	8.8	108	187 ± 17	0.18 ± 0.05	155 ± 3	12 ± 3	91

[a]For comparison, raw silica A200 data are included in the table. OM refers to organic mass content, IPA suspension data are for particle size, coating data are for water contact angle and surface roughness, see experimental section for details.

little dependent on the medium in which they are dispersed. This makes them easy-to-handle and adequate building blocks for the design of controlled rough surfaces.

3.1. Preparation of modified A200 with Tailored Size and Surface Energy. Controlled surface modification of silica nanoparticles is not trivial. The reaction conditions and reagents must be carefully chosen depending on the final purpose. Here, the target was the formation of small aggregates with the lowest possible surface energy. An oligodimethylsiloxane with short chain length was chosen as a modification agent to reduce the surface energy of the nanosilica. If longer chain lengths are used, then polymer bridges or entanglements can be formed between silica aggregates which leads to the formation of large agglomerates.[16] Physisorption instead of chemisorption was preferred because (i) the latter requires temperature and, sometimes, catalysts, which can promote self-condensation of the oligomers, and hence the uncontrolled increase of chain length and (ii) chemisorbed chains tend to lay perpendicular to the surface and then can be prone to the formation of bridges or entanglements, whereas physisorbed chains lay parallel to the silica surface.[25] Although experimental conditions to favor physisorption were chosen, the occurrence of chemically attached chains cannot be ruled out. The resulting P^7 is among the smallest aggregates that can be obtained by modification of A200 silica.[16] Table 1 gathers characterization data of the organosilica in comparison to A200 raw silica. These data support successful organic modification in P^7 particles. The OM% in P^7, amounting to almost 9%, is not negligible and the S_{BET} is reduced to almost half in comparison to the raw silica. On the basis of these data, the molar mass of the oligomer, and assuming a low self-condensation degree, the surface coverage can be calculated.[26,27] The number of molecules per nm^2 is around 0.6. This value is not high, but it must be taken into account that the reactant is an oligomer instead of a simple molecule. The structure of this organic coverage is then characterized by NMR.

Figure 1 compares the ^{29}Si and ^{13}C CP/MAS NMR spectra of the organosilica and the oligodimethylsiloxane used for surface reaction.

The P^7 ^{29}Si CP/MAS NMR spectrum is featured by the presence of two groups of signals assigned to the inorganic Q region from −105 to −120 ppm, absent in the oligomer spectrum, and the organic D region from −20 to 0 ppm.[28,29] The latter spectral region is strongly affected by the chain length and arrangement of the dimethylsiloxane due to the influence of the Si—O—Si bond geometry on ^{29}Si chemical shifts, which makes it very useful for structural elucidation.[25,30] The PDMS-7 signal located at around −12 ppm, is assigned to chain ends (silanols).[25,29] This component also detected in P^7 is a sign of the chain attachment onto the silica by physisorption and not by chemisorption, which involves condensation between the PDMS silanols and those on the surface. However, the component at −22 ppm, the only signal

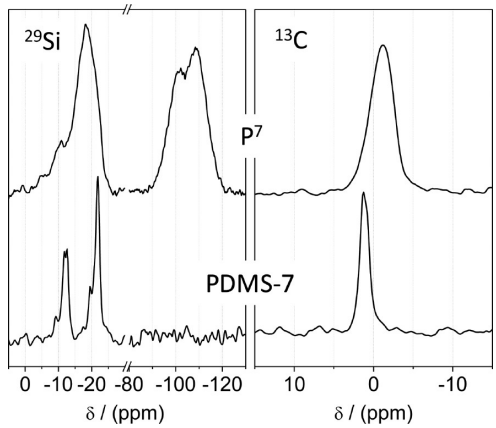

Figure 1. ^{29}Si (left) and ^{13}C (right) CP/MAS NMR spectra of organosilica P^7 and the reagent used in the modification reaction: the oligodimethylsiloxane PDMS-7.

in long chain PDMS,[25] associated with free siloxane units, is observed in the PDMS-7 spectrum but is undetectable in P^7. The organosilica presents a main signal located at around −19 ppm, which is assigned to siloxane units in a constrained environment.

The ^{29}Si data are supported by the methyl signal in the P^7 ^{13}C CP/MAS NMR spectrum which is broader and downshifted compared to PDMS-7, indicating a close contact with the silica surface.[16] In summary, the NMR data suggest the existence of physisorbed short polymer chains parallel to the silica surface.[25] This is exactly the desired scenario to lower the surface energy while avoiding the formation of chemical or physical bridges between silica aggregates.

This particular structure of the organic coverage is reflected in the behavior in suspension. Once dispersed in IPA, P^7 particles result in Z_{ave} values lower than those of A200 in the same solvent (see Table 1). This size reduction is explained by the release of the strong particle−particle interactions in raw silica by the introduction of the low surface energy reagent, and the absence of additional interactions (bridging or entanglements) between silica aggregates via this reagent. The Pdi is low, indicating a relatively narrow size distribution for this kind of silica.

Thus, the modification procedure gives rise to low surface energy P^7 silica particles organized into small aggregates. Although the size of P^7 is smaller than the neat A200, the autosimilar morphology of the latter is not lost in the former. This is essential, as it has been proved that autosimilar morphology provides an optimum surface roughness for the development of antiwetting behavior.[31] These modified particles are then used to prepare coatings on different supports.

3.2. Coating of Macro and Microsurfaces based on Neat P^7 Suspensions. *3.2.1. Glass, Plastic, and Paper.*

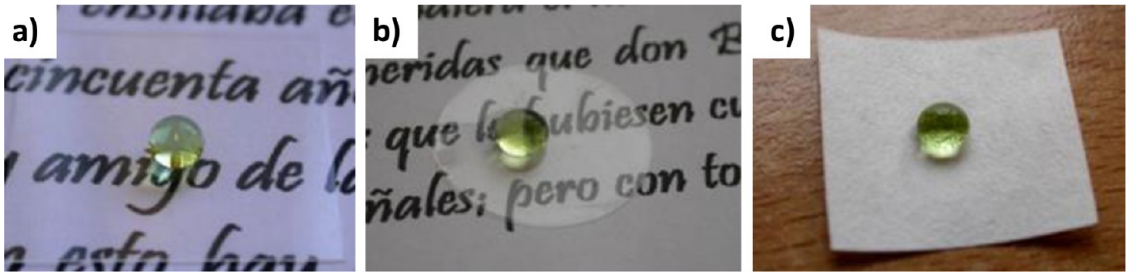

Figure 2. Images showing the appearance of P^7 coatings on a (a) glass support, (b) PMMA film, and (c) Whatman filter paper.

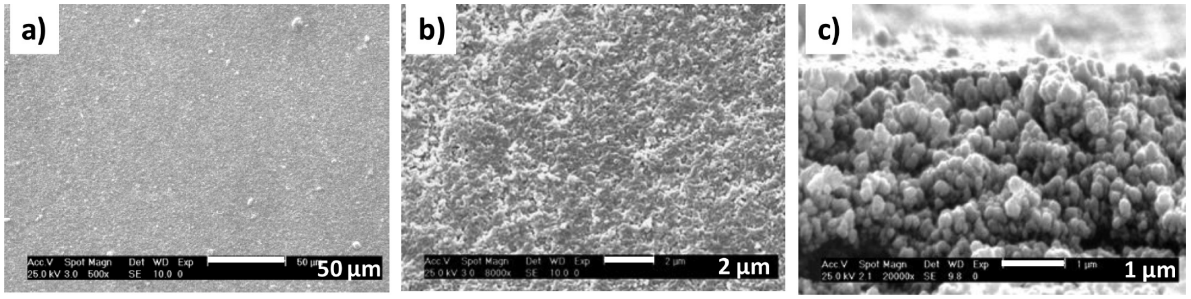

Figure 3. SEM images of the P^7 coating on a glass support: (a) and (b) surface, and (c) cross section.

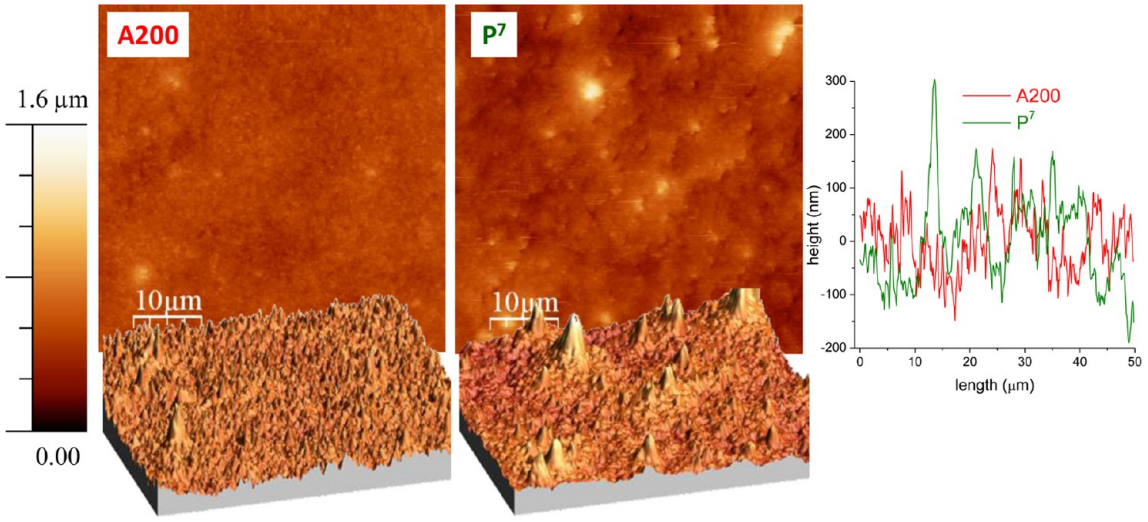

Figure 4. AFM images (2D and 3D) of A200 and P^7 coatings at 50 × 50 μm^2 and representative cross sections taken from these surfaces.

Figure 2 collects the pictures of a tinted drop of water on a glass support, a PMMA film, and a Whatman filter paper coated with P^7 deposited from an IPA suspension. The surfaces are highly hydrophobic, close to superhydrophobicity, see Table 1. Water contact angle and hysteresis seem to be independent of the support, as coatings on paper and plastic show very similar values to those shown for glass. However, while the surface wetting properties are profoundly altered by the P^7 coating, other characteristic properties of the supports remain unchanged. Thus, glass and PMMA film preserve transparency and are glossy, whereas the filter paper becomes waterproof. The P^7 coating is "invisible" and imperceptible in all the supports. To comprehend the reason behind the combination of hydrophobicity and optical transparency, it is worthwhile to study surface topography.

Figure 3 shows SEM images of the P^7 coating on a glass support. The coating is homogeneous and continuous (Figure 3a). This is important in order to achieve a low $\Delta\theta$ value. At higher magnification, it is possible to distinguish the particulate morphology of the coating (Figure 3b), while inspection of the section (Figure 3c) reveals that the coating is composed of globular entities of about 0.2 μm in diameter. A notable and advantageous feature of the coating is that the morphology is the same along the whole section. The wetting behavior is then expected to prevail in the case of wear or peeling off of the exterior layers.

Figure 4 includes AFM images[32] and cross sections of A200 and P^7 coatings on glass substrates prepared under the same conditions. Coatings of both A200 and P^7 are smooth at the microscale, and display a continuous roughness at the nanoscale. In P^7, the combination of low surface energy and sufficient nanoscale roughness, of dimensions well under that of visible light wavelength, produces a coating which is both ultrahydrophobic and transparent.

The P^7 AFM image reveals the existence of some peaks which are absent in the smoother A200. This is clearly

quantified by the difference in Rq listed in Table 1. The aggregate size registered in suspension (Table 1) fits well with the entities observed by SEM imaging and the AFM roughness profile. This strongly suggests that the morphology and size of the organosilica in suspension is transferred into the coating.

Although A200 presents discrete aggregates in IPA suspension, once deposited on a support, they can pack efficiently, blurring the boundaries between them by their mutual interpenetration, resulting in a smooth surface. This is not possible for P^7, since the surface modification has the effect of more clearly defining the boundaries between the aggregates, which become "harder" and cannot fuse with each other, what is translated into the surface roughness. This phenomenon is charted in Scheme 1 and is the basis of what we have termed "chemically guided topography".[16,17]

Scheme 1. A200 and P^7 Coatings from Suspensions

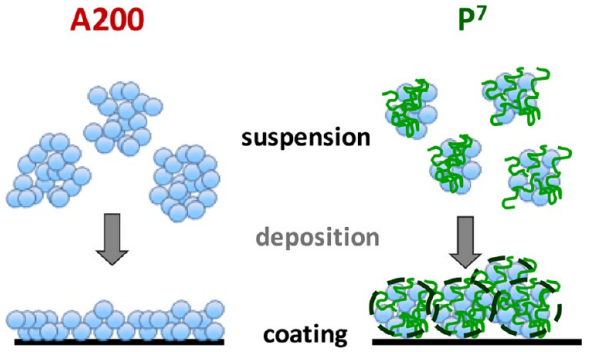

Care has to be taken to select the derivatization reagent and reaction conditions to modify the silica "enough but not too much". "Enough" to lower the surface energy sufficiently, but "not too much", in order to (i) maintain the autosimilar morphology of parent A200 aggregates, which is responsible for the final surface roughness and positively influences hydrophobicity, and (ii) to avoid the formation of huge aggregates/agglomerates which will compromise the continuity of the coating and, thus, its transparency and hysteresis. The final consequence is that P^7 coating shows very favorable antiwetting properties. The fact that P^7 coatings do not quite reach superhydrophobicity can be due to either a surface energy that is not low enough or to a surface roughness which is not sufficiently high, although the factors are difficult to decouple.

3.2.2. Coating of P^7 on Cellulose Microfibrils. Along the years, different strategies have been explored to hydrophobize cellulose fibers. As paradigmatic examples, we could cite the vapor deposition of silanes,[33,34] the chemical or physical adsorption of particles to modify the surface energy and roughness,[35−40] or the adsorption of polymers.[41,42] However, a method which combines a fluorine-free chemistry and a simple or one-step approach is not as common. With the intention of pointing out the versatility of the method, P^7 particles have been utilized to coat not only macroscopic surfaces as in Figure 2, but also microscopic surfaces such as those of NFC. To do so, a facile and rapid approach is employed in this work: the starting material was an NFC aerogel which was immersed in IPA dispersions of P^7 at three different particle concentrations: 0.1, 0.6, and 3 wt % (NFC-0.1, NFC-0.6, and NFC-3 hereafter). SEM images of the parent and modified aerogels appear in Figure 5.

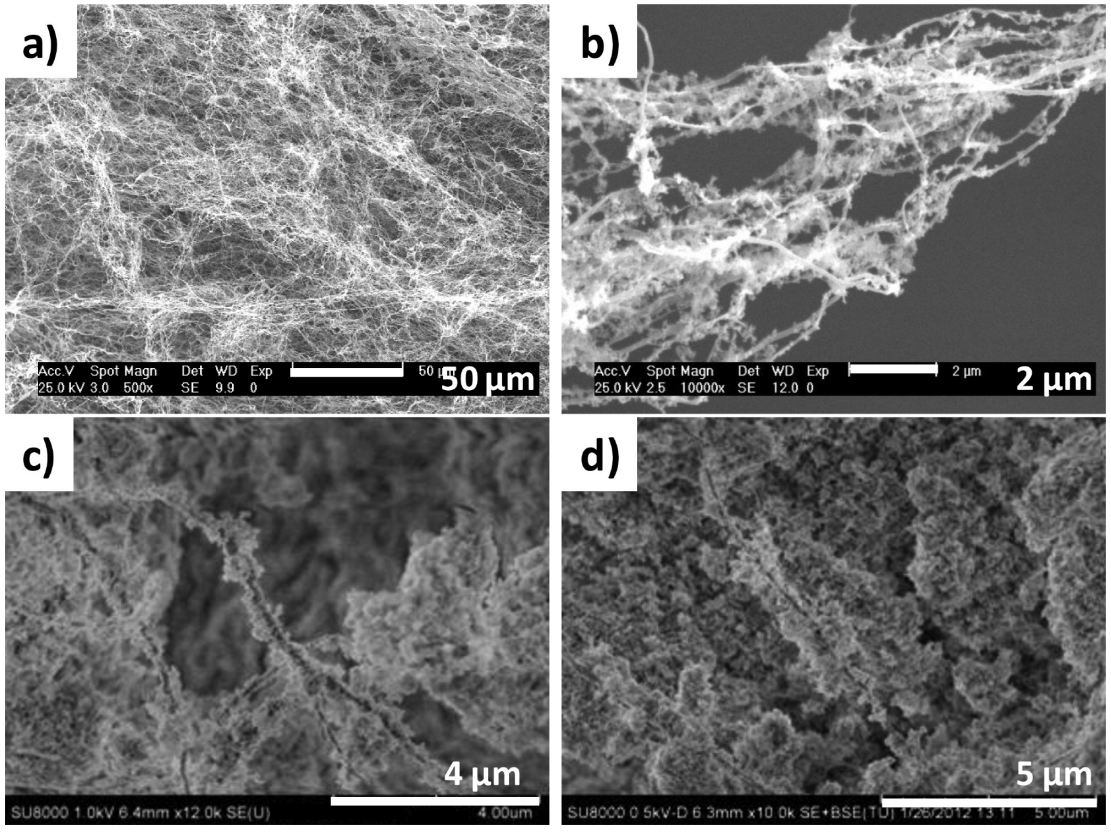

Figure 5. SEM images of (a) NFC, (b) NFC-0.1, (c) NFC-0.6, and (d) NFC-3.

In the three resulting aerogels, the organosilica P^7 is localized at the surface of the fibers. The interaction between P^7 and NFC seems to be very good, and a large number of particles coat the fibrils. Cellulose nanofibrils become covered by particle aggregates and are not seen as isolated entities in NFC-3, the material with the highest content of particles. In NFC-0.6, fibrils appear individualized, and finally NFC-0.1 is composed of well separated particle-coated NFC. The thickness of the particle coating is not easily quantified but roughly ranged between 300 and 400 nm for NFC-0.1 to 800 nm for NFC-3.

In the same way as the surfaces on the preceding section are made hydrophobic by their coating with P^7, it is expected that the aerogel composed of NFC coated with P^7 is also hydrophobic. To test the level of hydrophobization imparted by this procedure, the modified aerogels were immersed in water and their behavior was compared to that of the parent NFC aerogel. While the NFC aerogel disaggregates as soon as it comes into contact with water, NFC-0.1 floats and does not lose integrity even after long immersion times (pictures shown in Figure S1 of the Supporting Information, SI). Therefore, this simple and rapid approach is suitable for the hydrophobization of this kind of aerogels. The materials can be used as such or be subsequently processed to produce cellulose-based materials.

4. Superhydrophobic Polymer/P^7 Coatings. In the preceding section, different materials are coated with a P^7 layer, which successfully makes the different substrates highly hydrophobic. There are very small differences in terms of application procedure for the P^7 suspension to the surface of a glass, plastic, or paper surface, or to the cellulose aerogels. In all cases, the procedure consists in putting the substrate in contact with the suspension, either by spraying or by dipping. However, a crucial difference exists in the mechanical stability of the hydrophobic NFC aerogel in comparison with the other cases. The adhesion and interactions between P^7 and NFC seem to be strong (supported by literature data on adsorption of silica particles[38−40] and PDMS[41]), while the interaction of P^7 with macroscopically rough surfaces is much weaker, as expected. This low interaction and low adhesion results in poor mechanical stability of the P^7 coatings deposited on macro-surfaces. For many cases, this will limit practical applications. The provision of good mechanical stability to the coatings motivates the second methodology presented in this work, the preparation of superhydrophobic polymer/P^7 composite coatings.

4.1. Superhydrophobic PMMA/P^7 Composite Coatings. Preservation of the P^7 topography and transparency and introduction of sufficient binding properties to impart mechanical stability has been thoroughly investigated.[17] Using PMMA as binder, it is possible to produce a coating easily applied by spraying which combines the three properties discussed above. Although it can be considered as hydrophilic, since its θ_w is lower than 90° (θ_w = 68°), PMMA was chosen as a polymer matrix because of its mechanical and optical properties and because it allows high content of silica particles.[24] As a matter of fact, not being hydrophobic, PMMA is an optimum choice to illustrate this methodology.

To test the performance of the P^7 particles in combination with the polymer, we compared two composite coatings prepared with A200 raw silica (A200-50-PMMA) and P^7 organosilica (P^7-50-PMMA) with PMMA at a 50/50 wt % ratio. Table 2 collects the surface characterization data and Figure 6 graphical information on these coatings.

Table 2. Surface Characterization of the Coatings Prepared with A200 and P^7 and PMMA in a Ratio (50/50 wt %)

coating	description	θ_w (deg)	$\Delta\theta$ (deg)	Rq50 (nm)
A200-50-PMMA	raw silica/PMMA (50/50 wt %)	144 ± 1	>20	269
P^7-50-PMMA	P^7/PMMA (50/50 wt %)	157 ± 3	10 ± 1	166

In spite of containing the same particle content, the two coatings have very different appearance. PMMA interacts with the A200 surface, leading to large particle agglomerates as a consequence of the close contact between aggregates by polymer bridges.[16] This is translated into the sharp topography (high Rq value) and the opacity of the A200-50-PMMA coating (see Figure 6). On the contrary, P^7 particles do not agglomerate even in a good solvent for PDMS (toluene) (short PDMS chains are unable to form entanglement or polymer bridges between aggregates even when they are extended, i.e., in a good solvent) and give rise to a smooth P^7-50-PMMA coating, which preserves the transparency of the polymer matrix.

SEM images show a homogeneous and continuous coating in the case of P^7-50-PMMA, whereas A200-50-PMMA shows cracks. In A200-50-PMMA, most of the PMMA is involved in interactions with the particles. There is not enough non-interfacial polymer available to form a continuous film, and then, cracks appear.

Not only are the optical properties inferior for A200-50-PMMA, but also the wetting behavior is worse compared to P^7-50-PMMA. The high Rq value, the lack of homogeneity, and the presence of cracks have a detrimental effect on the contact angle and $\Delta\theta$. The data in Table 2 show that A200-50-PMMA is ultrahydrophobic (θ_w> 120°), but $\Delta\theta$ is difficult to measure because of its high value. In contrast, P^7-50-PMMA exhibits a wetting behavior that reaches superhydrophobicity. The resemblance between P^7 and P^7-50-PMMA coatings is very surprising, not only in their wetting behavior, but also in its particulate morphology, illustrated in the SEM image of the cross section in Figure 6. It is seems that the P^7 aggregate size prevails after mixing with the PMMA. Moreover, this morphology is also mechanically stable (see as example the coating on a flexible LDPE film included in Figure 6) and wear resistant, besides to superhydrophobic. Actually, scratch resistance was significantly improved with particle addition in comparison with PMMA, as will be presented in a separate study. Data in Tables 1 and 2 evidence that, compared with a neat P^7 coating, the introduction of a polymer matrix does not necessarily lead to a sacrifice in hydrophobicity.

This example shows the advantage of using well-controlled modified particles as hydrophobic agents. It also indicates the potential for multifunctional properties. For this reason, other polymer matrixes with different functionalities were also tested as particle binders.

4.2. Water Repellent Paint. P^7 has turned an intrinsically hydrophilic polymer such as PMMA into hydrophobic. Following a similar approach as that described for PMMA, a commercial acrylic car paint formulation was used as matrix to obtain a self-cleaning paint. In real life applications, the possibilities to fine-tune the chemistry of suspensions will be restricted. It is in this context that P^7 organosilica aggregates may have potential. They can be dispersed in many liquid media even by mild stirring or mixing conditions. P^7 mixing with the acrylic paint was carried out by magnetic stirring

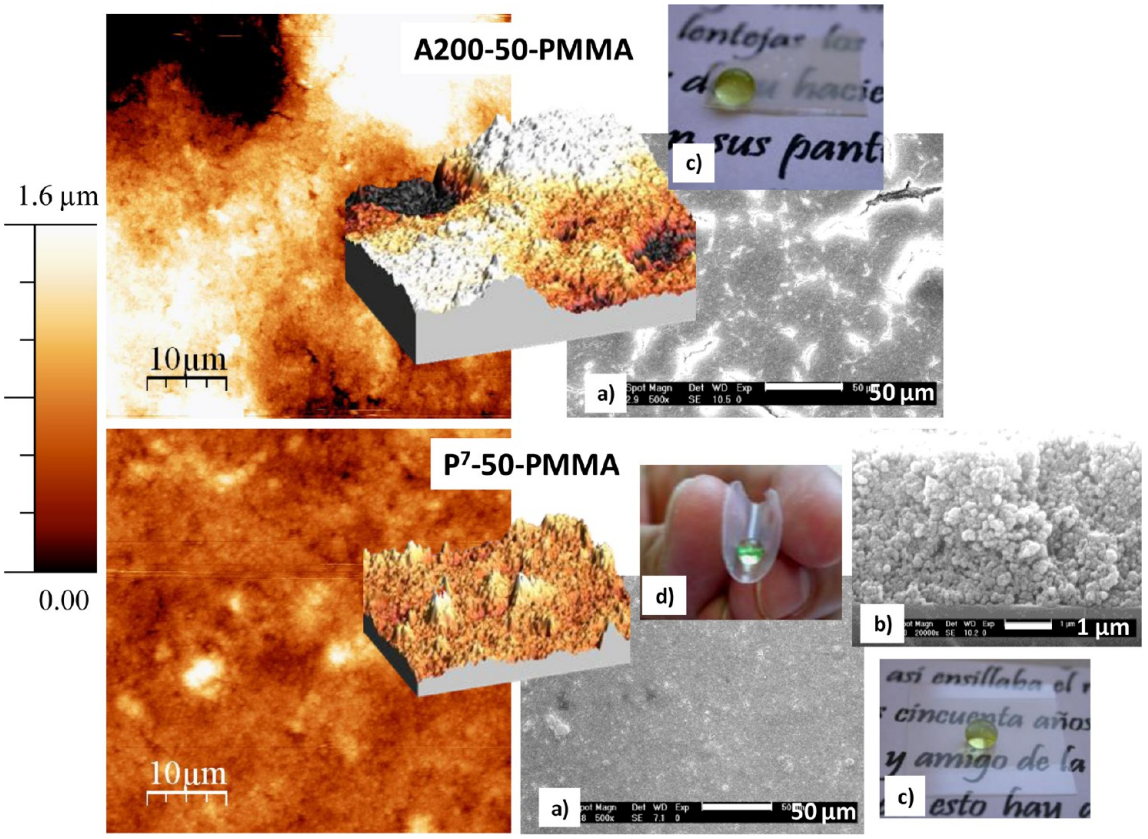

Figure 6. AFM data (2D and 3D images), SEM images of the surface (a) and cross-section (b), and pictures of the A200-50-PMMA (top) and P^7-50-PMMA (bottom) coatings on a glass support (c) (also included a picture of the latter on a PE film (d)).

during 3 and 24 h. Stirring time and rate are crucial parameters to understand the final surface roughness. Long stirring times and rates lead to the smoothing of the surface profile, probably because of the breaking down of particle agglomerates or even aggregates.[17] After mixing, the coating is deposited onto the support by spraying. The result is a coating with good adhesion to the support, and which can be handled without risk of damage. Table 3 collects the experimental conditions and resulting wetting properties of the commercial paint and the blends prepared.

Table 3. Preparation Conditions and Wetting Behavior of Composite Coatings Prepared from the Commercial Acrylic Paint and P^7

coating	P^7 (wt %)	stirring time (h)	θ_w (deg)	$\Delta\theta$ (deg)
acrylic paint	0	3	90 ± 1	>20
P^7-50-ACRY-1	50	3	162 ± 1	0
P^7-50-ACRY-2	50	24	145 ± 1	20 ± 2

The data in this table show that with a 50/50 wt % mixture of the matrix and particles, it is possible to induce a superhydrophobic behavior in a commercial paint without largely modifying their actual processing and application procedures. The coating named P^7-50-ACRY-1 shows pearl bouncing droplet behavior and the water droplets roll off the surface without any tilt angle (see videos and Figure S2 in the SI).

Besides the successful water repellency imparted by P^7, other interesting conclusions are derived from Table 3. Stirring time proves to be an important experimental parameter. Increased stirring time leads to a strong decrease in the antiwetting behavior in P^7-50-ACRY-2. Possibly, long stirring times reduces the P^7 aggregate size, which is a disadvantage since P^7 is already close to the size limit required for sufficient roughness.

Figure 7 shows AFM and SEM images of the paint, where the resemblance with the P^7 coating is noticeable, not only regarding the particulate morphology and the aggregate size but also to the roughness scale (Rq = 90 nm). This result suggests that the P^7 coating does not reach superhydrophobicity because of its surface energy is insufficiently low, and not because of the lack of roughness. The addition of a hydrophobic matrix (see θ_w in Table 3 for the acrylic paint) to P^7 increases hydrophobicity to the point of reaching pearl bouncing droplet behavior with the same roughness profile as the P^7 coating. However, P^7-50-PMMA, with the same particle content as P^7-50-ACRY-1, is less water repellent even with rougher profile (see Table 2) due to the hydrophilic nature of the PMMA.

Again, the particulate morphology of P^7-50-ACRY-1 (Figure 7) results in the same coating composition and structure through-the-thickness. Wear of outer layers should therefore not result in changes in the wetting behavior, a desirable feature for car paint applications.

4.3. Superhydrophobic and Luminescent PFO/P^7 composites. Addition of polymer binders to P^7 results in composite coatings of mechanical stability. Also, composite coatings can positively affect the hydrophobicity of the resulting surface. The next challenge is to study the potential to combine several other polymer functionalities. This was exemplified by choosing PFO, a luminescent polymer. PFO is a well-known conjugated polymer, which can be employed for the production of fluorescent sensors[43,44] because of its intense photolumines-

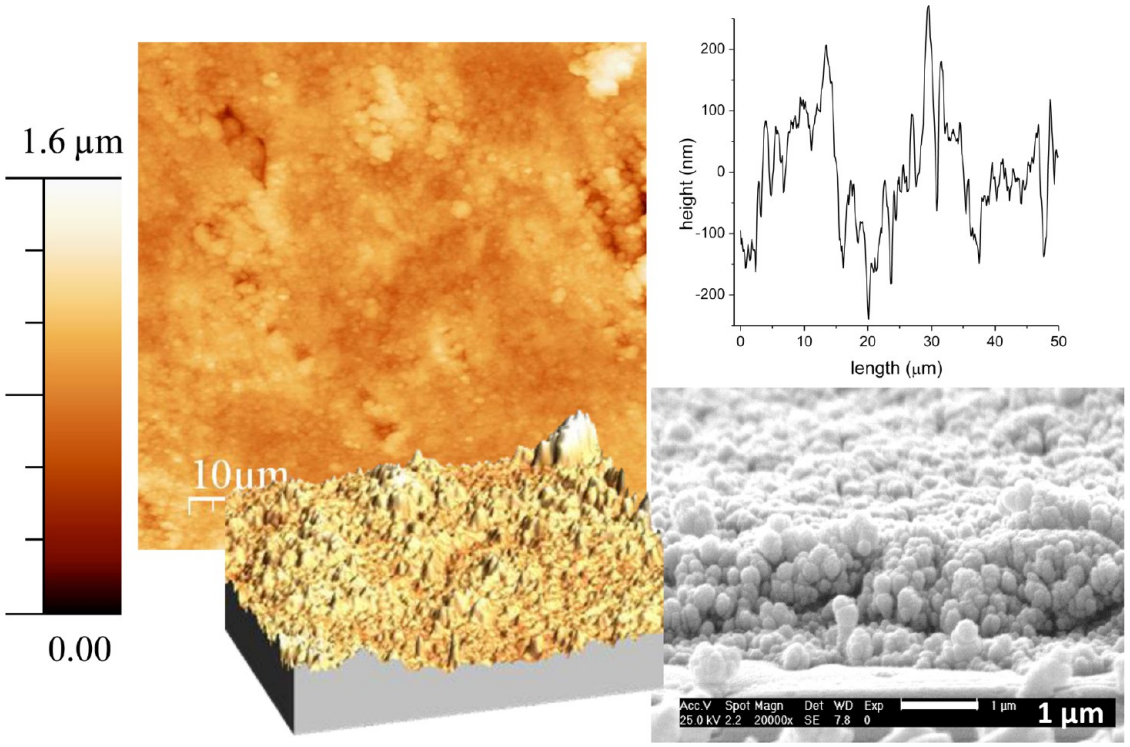

Figure 7. AFM data (2D and 3D images and cross section at 50 × 50 μm^2) and SEM image of the profile of the P^7-50-ACRY-1 painting.

cence. It is also very promising as molecular cable material, because of its good charge transport properties. This makes it become a powerful candidate for optoelectronics devices,[45] such as light emitting diodes (OLED)[46,47] or in organic photovoltaics (OPV).[48,49]

P^7 particles were added at several ratios (10, 30, and 50 wt % with respect to the polymer) to a PFO solution in toluene. After optimization, the selected stirring time was 24 h before depositing the mixture on different supports. Apart from glass, cellulose based membranes were used as supports, mainly due to the recent interest in cellulose as a flexible and sustainable substrate in optoelectronic applications.[50,51] One of the shortcomings associated with this support is its poor water resistance. This is the reason why superhydrophobicity would be a desirable additional feature. The coatings prepared and their wetting behavior are presented in Table 4.

PFO is a hydrophobic polymer (polycyclic aromatic hydrocarbon) with θ_w = 106° when deposited on a smooth support (glass) and θ_w = 135 and 151° when supported on porous substrate such as Whatman or cellulose membranes, respectively. Actually, PFO-C is a superhydrophobic coating since its hysteresis is under 10°. SEM images of these coatings at different magnifications are collected in Figure 8. Note that the use of different magnifications for the different supports provides important information with respect to the support and coating morphology. As expected PFO-G is a continuous and homogeneous coating, whereas PFO-C forms spherical particles on the surface of the cellulose membrane. This is because of the highly incompatible nature of the components: cellulose highly hydrophilic whereas PFO is a very hydrophobic aromatic hydrocarbon polymer. This peculiar morphology of polymer pearls on the porous substrate would be clearly related to the superhydrophobic behavior of this coating.

Some representative SEM images of selected PFO/P^7 coatings are collected in Figure S4 of the SI. The wetting

Table 4. Nomenclature, Substrate Type, Composition, and Wetting Behavior of PFO/P^7 Composites[a]

coating	substrate	P^7 wt %	θ_w (deg)	$\Delta\theta$ (deg)
P^7-G	glass	100	155 ± 3	12 ± 3
PFO-G	glass	0	106 ± 1	>20
P^7-10-PFO-G	glass	10	109 ± 1	18 ± 2
P^7-30-PFO-G	glass	30	157 ± 1	5 ± 2
P^7-50-PFO-G	glass	50	164 ± 2	3 ± 1
P^7-C	cellulose membrane	100	165 ± 2	13 ± 2
PFO-C	cellulose membrane	0	151 ± 4	9 ± 5
P^7-10-PFO-C	cellulose membrane	10	107 ± 2	>20
P^7-30-PFO-C	cellulose membrane	30	153 ± 1	5 ± 1
P^7-50-PFO-C	cellulose membrane	50	165 ± 3	0
P^7-W	Whatman	100	160 ± 2	15 ± 2
PFO-W	Whatman	0	135 ± 1	14 ± 4
P^7-10-PFO-W	Whatman	10	123 ± 1	>20
P^7-30-PFO-W	Whatman	30	150 ± 1	9 ± 4
P^7-50-PFO-W	Whatman	50	167 ± 1	2 ± 2

[a](P^7-X stands for particle-only coatings in the different supports, the same for PFO-X but with polymer-only coatings).

behavior presented in Table 4 can be understood by looking at the morphology of the surface. The 10 wt % containing composites do not show sufficient and continuous surface roughness to develop hydrophobicity; a coating with large smooth domains devoid of particles is seen. P^7-10-PFO-G shows an insignificant increase in θ_w and a detectable decrease in $\Delta\theta$. The pearl-like morphology observed in PFO-C is lost in the case of P^7-10-PFO-C, where the porous structure of the substrate is completely covered by the composite. This is the reason behind the loss of antiwetting properties. Polymer-only domains are still clearly smaller when increasing the particle content up to 30 wt %. The three coatings with this particle content (P^7-30-PFO-G, P^7-30-PFO-C, and P^7-30-PFO-W)

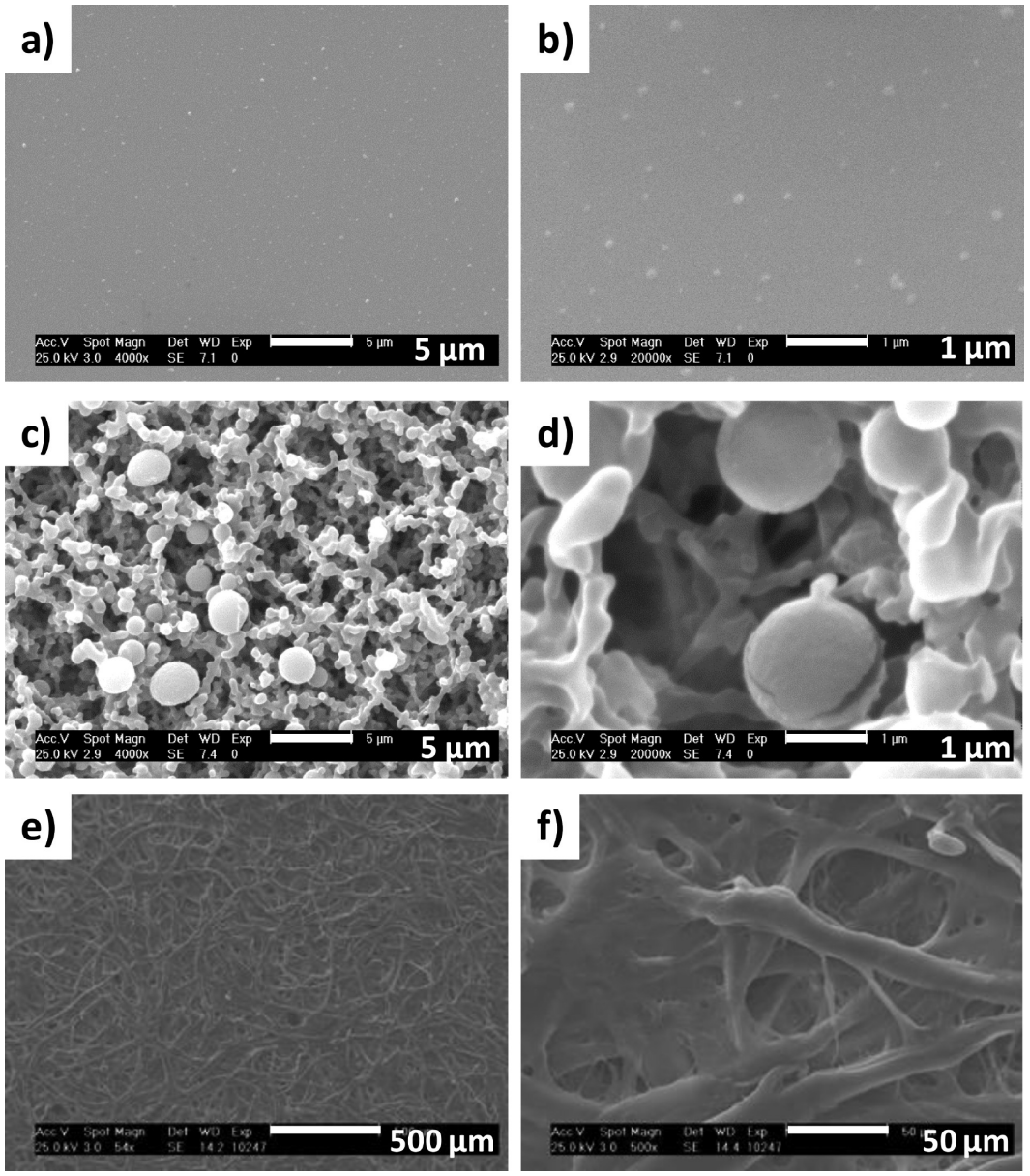

Figure 8. SEM micrographs of the coatings: (a) and (b) PFO-G, (c) and (d) PFO-C, and (e) and (f) PFO-W.

exhibit a rough surface morphology. The blend coats the pore walls and fibers in cellulose based supports, enhancing the roughness of the substrate. The consequence is an increase in water repellency, which reaches superhydrophobicity. Finally, composites containing 50 wt % of P^7 show an even rougher surface resembling that observed for the P^7 coating. As a consequence, all the coatings containing 50 wt % of P^7 particles are highly hydrophobic but P^7-50-PFO-C even achieves a pearl bouncing droplet behavior. AFM and SEM imaging of the surface topography of P^7-50-PFO-C coating appears in Figure 9.

The surface analysis reveals that, apart from the particulate morphology, this coating has developed a dual scale topography, a feature associated with PFO and not registered with the other polymer matrixes tested (PMMA and the paint). In the 50×50 μm^2 images, micrometric entities (more than 2 μm height as seen in the cross section) are observed, covered with the particulate morphology at the nanoscale. These micrometric structures induce an increase in Rq which in this coating is 485 ± 78 nm, well above those measured for the other particle/polymer systems described in preceding sections. This dual scale roughness was formerly thought to be essential for superhydrophobicity to develop. However, we have shown that the P^7 coating, P^7-50-PMMA, and P^7-50-ACRY-1 are almost superhydrophobic or superhydrophobic surfaces without a detectable roughness at the microscopic scale. As experimental conditions are practically identical when preparing the composites and coatings with the three polymer matrixes, the different topographies found must be caused by the nature of the interactions between P^7 and each of PMMA, acrylic paint, and PFO. The results suggest that the stronger these interactions the more likely that roughness at larger size scales will appear, due to P^7 agglomeration via interactions with the polymer binder. Note that the interactions of PMMA with the naked surface of A200 are stronger than with the modified surface of P^7 resulting in a rougher topography for A200-50-PMMA than in P^7-50-PMMA. Attending to the interaction criterion, the affinity scale of the polymer tested in this work

dx.doi.org/10.1021/am504886y | ACS Appl. Mater. Interfaces 2014, 6, 18998−19010

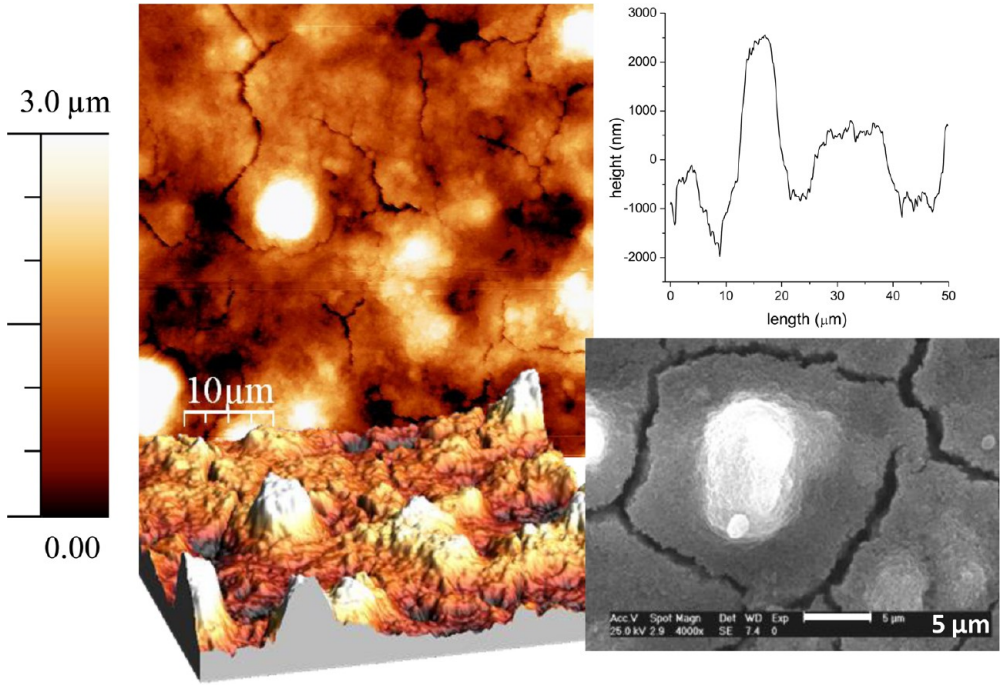

Figure 9. AFM data (2D, 3D, and cross section at 50 × 50 μm^2) and SEM image of the P^7-50-PFO-C coating.

and the P^7 would be PFO > PMMA > paint. This empirical evidence opens the window to the design of tailor-made surfaces tuned in terms on hydrophobicity, transparency, mechanical stability, and other functionalities.

The combination of superhydrophobicity and fluorescence, in particular in the P^7-50-PFO-W coating is illustrated in the video attached as SI (see also Figure S4). The video shows the coating under UV light and with water droplets rolling off its surface. While becoming superhydrophobic, PFO continues to absorb UV light at λ = 385 nm and to emit its characteristic blue fluorescence.[52−54]

CONCLUSIONS

Silica nanoparticles (A200) have been modified with oligodimethylsiloxane to form nonfluorinated ultrahydrophobic particle aggregates (termed P^7 organosilica) which are the basis of the present multipurpose antiwetting approach. These organosilica aggregates form stable colloidal suspensions in IPA and toluene, being their morphology and size quite independent of the suspension media. A simple but industrially scalable spraying process is used to prepare hydrophobic coatings from them. The coatings achieve ultrahydrophobicity (θ_w over 150° and $\Delta\theta$ within 10° and 13°) on glass, plastic or paper substrates. A related dipping approach is used to hydrophobize nanoporous cellulose aerogels, which are able to float on water.

Multifunctional polymer-based composite coatings incorporating high P^7 ratios have also been prepared, again by simple spraying. With PMMA, the coatings are at the limit of superhydrophobicity, being also quite transparent and mechanically stable. Likewise, self-cleaning paints are obtained when the organosilica particles are mixed with commercial acrylic car paint. With PFO, a hydrophobic and luminescent polymer, superhydrophobic and luminescent composite coatings on glass and cellulose based substrates have been developed.

In summary, industrially scalable materials and processing concepts were demonstrated for fluorine-free multipurpose coatings with ultra or superhydrophobic properties, where the control and stability of the organosilica aggregate dimensions and morphology are critical parameters.

ASSOCIATED CONTENT

Supporting Information

Images showing the behavior in water of NFC and NFC-0.1 (Figure S1), a sequence of frames illustrating the pearl bouncing droplet behavior of the paint: P^7-50-ACRY-1 (Figure S2), SEM micrographs of the coatings based on PFO/P^7 composites (Figure S3), and an example of the combination of superhydrophobicity and light emitting properties (Figure S3). In addition, videos showing the pearl bouncing droplet behavior of the paint, P^7-50-ACRY-1, and the superhydrophobicity and luminescence of the P^7-50-PFO-W. This material is available free of charge via the Internet at http://pubs.acs.org.

AUTHOR INFORMATION

Corresponding Authors

*E-mail: ptiemblo@ictp.csic.es.
*E-mail: ngarcia@ictp.csic.es.

Present Address

[⊥]Universidad de Alcalá, Facultad de Farmacia, Autovía A2, 33.600, 28871, Alcalá de Henares, Madrid, Spain.

Notes

The authors declare no competing financial interest.

ACKNOWLEDGMENTS

The authors acknowledge financial support from the Spanish Ministry via Project MAT2011-29174-C02-02 and CSIC (PIE200960I087, PIE 201160E109, and PIE201360E078). R.d.F. wants to thank CSIC for a grant through the JAE-Pre Program. M.H. and P.T. acknowledge the funding received from the People Programme (Marie Curie Actions) of the European Union's Seventh Framework Programme (FP7/2007-2013) under grant agreement no. PIIF-GA-2012-

327563.A.S. is thankful to DFG (Grants SY 125/1-1 and SY 125/4-1) for financial support.

REFERENCES

(1) Onda, T.; Shibuichi, S.; Satoh, N.; Tsujii, K. Super-Water-Repellent Fractal Surfaces. *Langmuir* **1996**, *12*, 2125−2127.
(2) Shibuichi, S.; Onda, T.; Satoh, N.; Tsujii, K. Super Water-Repellent Surfaces Resulting from Fractal Structure. *J. Phys. Chem.* **1996**, *100*, 19512−19517.
(3) Barthlott, W.; Neinhuis, C. Purity of the Sacred Lotus, or Escape from Contamination in Biological Surfaces. *Planta* **1997**, *202*, 1−8.
(4) Zhang, X.; Shi, F.; Niu, J.; Jiang, Y.; Wang, Z. Superhydrophobic Surfaces: From Structural Control to Functional Application. *J. Mater. Chem.* **2008**, *18*, 621−633.
(5) Nosonovsky, M.; Bhushan, B. Superhydrophobic Surfaces and Emerging Applications: Non-Adhesion, Energy, Green Engineering. *Curr. Opin. Colloid Interface Sci.* **2009**, *14*, 270−280.
(6) Cao, L.; J, A. K.; Sikka, V. K.; Wu, J.; Gao, D. Anti-icing superhydrophobic coatings. *Langmuir* **2009**, *25*, 12444−12448.
(7) Yao, X.; Song, Y.; Jiang, L. Applications of Bio-Inspired Special Wettable Surfaces. *Adv. Mater.* **2011**, *23*, 719−34.
(8) He, Z.; Ma, M.; Lan, X.; Chen, F.; Wang, K.; Deng, H.; Zhang, Q.; Fu, Q. Fabrication of a Transparent Superamphiphobic Coating with Improved Stability. *Soft Matter* **2011**, *7*, 6435.
(9) Xu, L.; Karunakaran, R. G.; Guo, J.; Yang, S. Transparent, Superhydrophobic Surfaces from One-Step Spin Coating of Hydrophobic Nanoparticles. *ACS Appl. Mater. Interfaces* **2012**, *4*, 1118−1125.
(10) Roach, P.; Shirtcliffe, N. J.; Newton, M. I. Progress in Superhydrophobic Surface Development. *Soft Matter* **2008**, *4*, 224−240.
(11) Ming, W.; Wu, D.; Van Benthem, R.; De With, G. Superhydrophobic Films from Raspberry-like Particles. *Nano Lett.* **2005**, *5*, 2298−2301.
(12) Verho, T.; Bower, C.; Andrew, P.; Franssila, S.; Ikkala, O.; Ras, R. H. A. Mechanically Durable Superhydrophobic Surfaces. *Adv. Mater.* **2011**, *23*, 673−678.
(13) Zhu, X.; Zhang, Z.; Men, X.; Yang, J.; Wang, K.; Xu, X.; Zhou, X.; Xue, Q. Robust Superhydrophobic Surfaces with Mechanical Durability and Easy Repairability. *J. Mater. Chem.* **2011**, *21*, 15793−15797.
(14) Cho, K. L.; Liaw, I. I.; Wu, A. H. F.; Lamb, R. N. Influence of Roughness on a Transparent Superhydrophobic Coating. *J. Phys. Chem. C* **2010**, *114*, 11228−11233.
(15) Guo, Z.; Liu, W. Biomimic from the Superhydrophobic Plant Leaves in Nature: Binary Structure and Unitary Structure. *Plant Sci.* **2007**, *172*, 1103−1112.
(16) Garcia, N.; Benito, E.; Tiemblo, P.; Hasan, M. M. B.; Synytska, A.; Stamm, M. Chemically Guided Topography in Alkylsilane- and Oligosiloxane-Modified Silica Nanoparticle Coatings: From very Hydrophobic Surfaces to "Pearl" Bouncing Droplets. *Soft Matter* **2010**, *6*, 4768−4776.
(17) De Francisco, R. PhD. Thesis. Universidad Autónoma de Madrid, 2013.
(18) Manoudis, P. N.; Karapanagiotis, I.; Tsakalof, A.; Zuburtikudis, I.; Panayiotou, C. Superhydrophobic Composite Films Produced on Various Substrates. *Langmuir* **2008**, *24*, 11225−11232.
(19) Wang, J.; Chen, X.; Kang, Y.; Yang, G.; Yu, L.; Zhang, P. Preparation of Superhydrophobic Poly(methyl methacrylate)-Silicon Dioxide Nanocomposite Films. *Appl. Surf. Sci.* **2010**, *257*, 1473−1477.
(20) Xu, L.; Gao, L.; He, J. Fabrication of Visible/Near-IR Antireflective and Superhydrophobic Coatings from Hydrophobically Modified Hollow Silica Nanoparticles and Poly(Methyl Methacrylate). *RSC Adv.* **2012**, *2*, 12764−12769.
(21) Joshi, S.; Fair, J. R. Adsorptive Drying of Toluene. *Ind. Eng. Chem. Res.* **1988**, *27*, 2078−2085.
(22) Henriksson, M.; Henriksson, G.; Berglund, L. A.; Lindström, T. An Environmentally Friendly Method for Enzyme-Assisted Preparation of Microfibrillated Cellulose (MFC) Nanofibers. *Eur. Polym. J.* **2007**, *43*, 3434−3441.
(23) Nielsen, K. T.; Bechgaard, K.; Krebs, F. C. Removal of Palladium Nanoparticles from Polymer Materials. *Macromolecules* **2005**, *38*, 658−659.
(24) Garcia, N.; Corrales, T.; Guzman, J.; Tiemblo, P. Understanding the Role of Nanosilica Particle Surfaces in the Thermal Degradation of Nano Silica-Poly(Methyl Methacrylate) Solution-Blended Nanocomposites: From Low to High Silica Concentration. *Polym. Degrad. Stab.* **2007**, *92*, 635−643.
(25) Litvinov, V. M.; Barthel, H.; Weis, J. Structure of a PDMS Layer Grafted onto a Silica Surface Studied by Means of DSC and Solid-State NMR. *Macromolecules* **2002**, *35*, 4356−4364.
(26) Berendsen, G. E.; de Galan, L. Preparation and Chromatographic Properties of some Chemically Bonded Phases for Reversed-Phase Liquid Chromatography. *J. Liq. Chromatogr* **1978**, *1*, 561−586.
(27) Garcia, N.; Benito, E.; Guzman, J.; Tiemblo, P. Use of *p*-Toluenesulfonic Acid for the Controlled Grafting of Alkoxysilanes onto Silanol Containing Surfaces: Preparation of Tunable Hydrophilic, Hydrophobic, and Superhydrophobic Silica. *J. Am. Chem. Soc.* **2007**, *129*, 5052−5060.
(28) Sindorf, D. W.; Maciel, G. E. Silicon-29 CP/MAS NMR Studies of Methylchlorosilane Reactions on Silica Gel. *J. Am. Chem. Soc.* **1981**, *103*, 4263−4265.
(29) Albert, K.; Bayer, E. Characterization of Bonded Phases by Solid-State NMR Spectroscopy. *J. Chromatogr. A* **1991**, *544*, 345−370.
(30) Babonneau, F. Hybrid Siloxane-Oxide Materials via Sol-Gel Processing: Structural Characterization. *Polyhedron* **1994**, *13*, 1123−1130.
(31) Schaefer, D. W.; Kohls, D.; Feinblum, E. Morphology of Highly Dispersing Precipitated Silica: Impact of Drying and Sonication. *J. Inorg. Organomet. Polym. Mater.* **2012**, *22*, 617−623.
(32) Horcas, I.; Fernández, R.; Gómez-Rodríguez, J. M.; Colchero, J.; Gómez-Herrero, J.; Baro, A. M. WSXM: A Software for Scanning Probe Microscopy and a Tool for Nanotechnology. *Rev. Sci. Instrum.* **2007**, *78*, Article. no. 013705.
(33) Cunha, A. G.; Freire, C.; Silvestre, A.; Pascoal Neto, C.; Gandini, A.; Belgacem, M. N.; Chaussy, D.; Beneventi, D. Preparation of Highly Hydrophobic and Lipophobic Cellulose Fibers by a Straightforward Gas-Solid Reaction. *J. Colloid Interface Sci.* **2010**, *344*, 588−595.
(34) Jin, H.; Kettunen, M.; Laiho, A.; Pynnönen, H.; Paltakari, J.; Marmur, A.; Ikkala, O.; Ras, R. H. A. Superhydrophobic and Superoleophobic Nanocellulose Aerogel Membranes as Bioinspired Cargo Carriers on Water and Oil. *Langmuir* **2011**, *27*, 1930−1934.
(35) Goncalves, G.; Marques, P. A.; Trindade, T.; Neto, C. P.; Gandini, A. Superhydrophobic Cellulose Nanocomposites. *J. Colloid Interface Sci.* **2008**, *324*, 42−46.
(36) Shateri Khalil-Abad, M.; Yazdanshenas, M. E. Superhydrophobic Antibacterial Cotton Textiles. *J. Colloid Interface Sci.* **2010**, *351*, 293−298.
(37) Korhonen, J. T.; Kettunen, M.; Ras, R. H. A.; Ikkala, O. Hydrophobic Nanocellulose Aerogels as Floating, Sustainable, Reusable, and Recyclable Oil Absorbents. *ACS Appl. Mater. Interfaces* **2011**, *3*, 1813−1816.
(38) Leng, B.; Shao, Z.; De With, G.; Ming, W. Superoleophobic Cotton Textiles. *Langmuir* **2009**, *25*, 2456−2460.
(39) Chen, X.; Liu, Y.; Lu, H.; Yang, H.; Zhou, X.; Xin, J. H. In-situ Growth of Silica Nanoparticles on Cellulose and Application of Hierarchical Structure in Biomimetic Hydrophobicity. *Cellulose* **2010**, *17*, 1103−1113.
(40) Shi, Y.; Wang, Y.; Feng, X.; Yue, G.; Yang, W. Fabrication of Superhydrophobicity on Cotton Fabric by Sol-Gel. *Appl. Surf. Sci.* **2012**, *258*, 8134−8138.
(41) Kim, D. H.; Kim, Y. S.; Wu, J.; Liu, Z.; Song, J.; Kim, H. S.; Huang, Y. Y.; Hwang, K. C.; Rogers, J. A. Ultrathin Silicon Circuits with Strain-Isolation Layers and Mesh Layouts for High-Performance Electronics on Fabric, Vinyl, Leather, and Paper. *Adv. Mater.* **2009**, *21*, 3703−3707.
(42) Aarne, N.; Laine, J.; Hänninen, T.; Rantanen, V.; Seitsonen, J.; Ruokolainen, J.; Kontturi, E. Controlled Hydrophobic Functionaliza-

tion of Natural Fibers Through Self-Assembly of Amphiphilic Diblock Copolymer Micelles. *ChemSusChem* **2013**, *6*, 1203−1208.
(43) Xu, H.; Wu, H.; Fan, C.; Li, W.; Zhang, Z.; He, L. Highly Sensitive Biosensors based on Water-Soluble Conjugated Polymers. *Chin. Sci. Bull.* **2004**, *49*, 2227−2231.
(44) Qin, C.; Tong, H.; Wang, L. Water-Soluble Phosphate-Functionalized Polyfluorene as Fluorescence Biosensors Toward Cytochrome C. *Sci. China, Ser. B: Chem.* **2009**, *52*, 833−839.
(45) Chen, P.; Yang, G.; Liu, T.; Li, T.; Wang, M.; Huang, W. Optimization of Opto-Electronic Property and Device Efficiency of Polyfluorenes by Tuning Structure and Morphology. *Polym. Int.* **2006**, *55*, 473−490.
(46) Wu, S. H.; Huang, H. M.; Chen, K. C.; Hu, C. W.; Hsu, C. C.; Tsiang, R. C. C. A Green Polymeric Light-Emitting Diode Material: Poly(9,9-dioctylfluorene-alt-thiophene) End-Capped with Gold Nanoparticles. *Adv. Funct. Mater.* **2006**, *16*, 1959−1966.
(47) Köhnen, A.; Irion, M.; Gather, M. C.; Rehmann, N.; Zacharias, P.; Meerholz, K. Highly Color-Stable Solution-Processed Multilayer WOLEDs for Lighting Application. *J. Mater. Chem.* **2010**, *20*, 3301−3306.
(48) Topham, P. D.; Parnell, A. J.; Hiorns, R. C. Block Copolymer Strategies for Solar Cell Technology. *J. Polym. Sci., Part B: Polym. Phys.* **2011**, *49*, 1131−1156.
(49) Lindgren, L. J.; Zhang, F.; Andersson, M.; Barrau, S.; Hellström, S.; Mammon, W.; Perzpn, E.; Inganäs, O.; Andersson, M. R. Synthesis, Characterization, and Devices of a Series of Alternating Copolymers for Solar Cells. *Chem. Mater.* **2009**, *21*, 3491−3502.
(50) Zhu, H.; Xiao, Z.; Liu, D.; Li, Y.; Weadock, N. J.; Fang, Z.; Huang, J.; Hu, L. Biodegradable Transparent Substrates for Flexible Organic-Light-Emitting Diodes. *Energy Environ. Sci.* **2013**, *6*, 2105−2111.
(51) Zhou, Y.; Fuentes-Hernandez, C.; Khan, T. M.; Liu, J. C.; Hsu, J.; Shim, J. W.; Dindar, A.; Youngblood, J. P.; Moon, R. J.; Kippelen, B. Recyclable Organic Solar Cells on Cellulose Nanocrystal Substrates. *Sci. Rep.* **2013**, *3*, Article no. 1536.
(52) Fukuda, M.; Sawada, K.; Yoshino, K. Synthesis of Fusible and Soluble Conducting Polyfluorene Derivatives and their Characteristics. *J. Polym. Sci., Part A: Polym. Chem.* **1993**, *31*, 2465−2472.
(53) Neher, D. Polyfluorene Homopolymers: Conjugated Liquid-Crystalline Polymers for Bright Blue Emission and Polarized Electroluminescence. *Macromol. Rapid Commun.* **2001**, *22*, 1365−1385.
(54) Scherf, U.; List, E. J. W. Semiconducting Polyfluorenes - Towards Reliable Structure-Property Relationships. *Adv. Mater.* **2002**, *14*, 477−487.